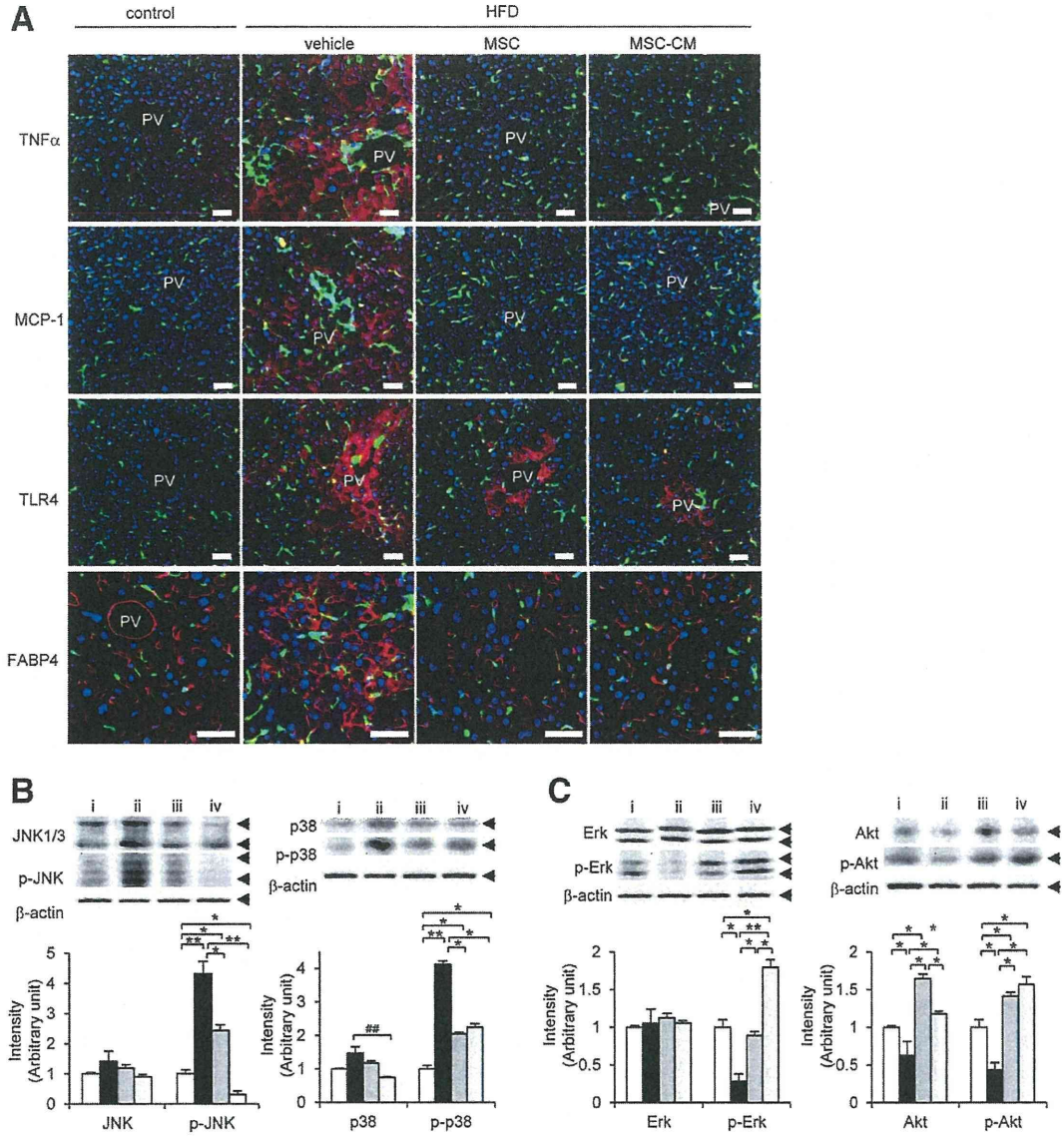

Fig. 5. Anti-inflammatory, proliferative, and antiapoptotic effects of rMSCs and rMSC-CM therapies in liver of HFD-diabetic mice. (A) Immunofluorescence staining (red) of TNFα, MCP-1, TLR4, and FABP4 in the liver. Bar, 50 μm. Protein levels of (B) JNK1/3, phosphorylation of JNK (p-JNK), p38-MAPK, phosphorylation of p38-MAPK (p-p38), (C) Erk1/2, p-Erk, Akt, and p-Akt in liver of mice in each group. (D) Photomicrographs of representative sections of the TUNEL reaction. The apoptotic index is quantified in right panel (mean value of 20 panels per group). (E) Protein levels of Bax, Bcl2, caspase-3, and cleaved caspase-3 in liver of mice in each group. Relative amounts of protein are normalized to an internal control, β-actin. Intensity is shown as an arbitrary unit (n = 5, each group). Data are expressed as mean ± SE values $*P < 0.05$; $**P < 0.01$.

MSC and MSC-CM Therapies Suppressed Apoptosis of Hepatocytes in HFD-Diabetic Mice and Enhanced Regeneration of Damaged Hepatocytes in STZ-Diabetic Mice. MSC and MSC-CM therapies markedly decreased terminal deoxynucleotidyl transferase-mediated dUTP nick end labeling (TUNEL)-positive cells in liver of HFD-diabetic mice (Fig. 5D). Mitochondria control cell fate by apoptosis-related molecules, such as Bax and B-cell lymphoma 2 (Bcl2), and the subsequent activation of caspase-3. The results showed that expression of Bax and cleaved caspase-3 was significantly increased in liver of HFD-vehicle mice. In addition, Bcl2 expression was significantly decreased in liver of HFD-vehicle mice. These alterations were reversed by MSC and MSC-CM therapies (Fig. 5E). On the other hand, expression of hepatocyte nuclear factor 4 (HNF-4) was stimulated, and the transcription factor, CCAAT/enhancer-binding protein alpha (C/EBPα), which was down-regulated in STZ-vehicle mice, was notably enhanced or recovered

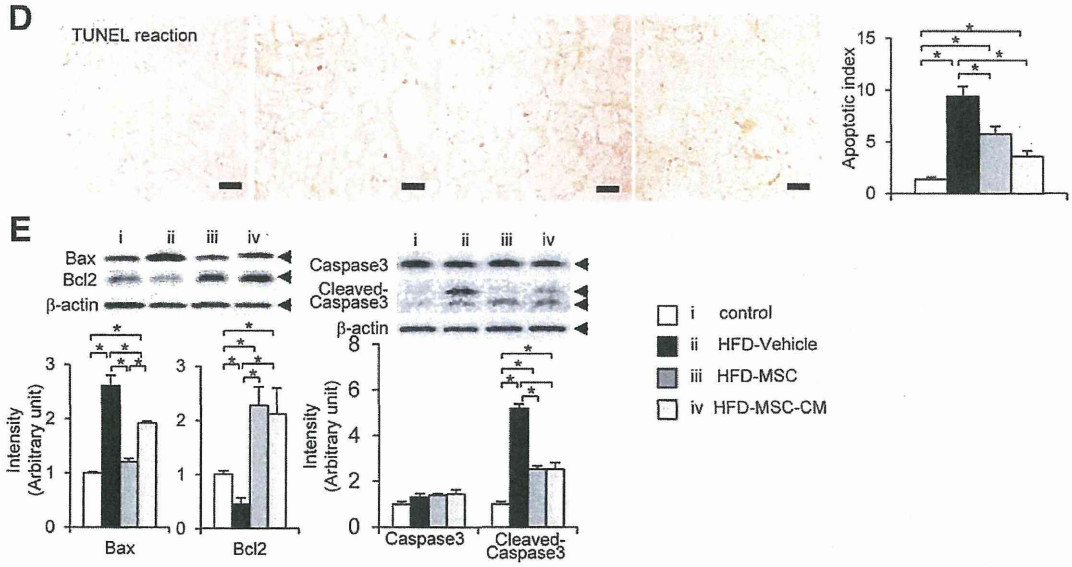

Fig. 5. (Continued)

by MSC and MSC-CM therapies (Fig. 6D). Expression of trophoblast cell-surface antigen 2 (also known as *Trop2*), which was remarkably decreased in STZ-vehicle mice, was recovered by MSC and MSC-CM therapies (Fig. 6E).

MSC and MSC-CM Therapies Prevented Lipogenesis, Fibrosis, Glucogenesis, and IR in Liver of HFD-Diabetic Mice. In HFD-vehicle mice, a number of large lipid droplets were precipitated in hepatocytes, but were decreased in both size and number in HFD-MSC and HFD-MSC-CM mice (Fig. 7A, top). Examination of Azan-stained sections revealed periportal fibrosis in HFD-vehicle mice (Fig. 7A, middle), which was suppressed by MSC and MSC-CM therapies. Expression of transforming growth factor beta 1 (TGF-β1), a marker of stellate cells, was increased in both resident cells and BMDCs in liver of HFD-vehicle mice, but was recovered by MSC and MSC-CM therapies (Fig. 7A, bottom).

Phosphorylation of insulin receptor substrate 2 (p-Irs2) serine and sterol response element-binding protein 1c (SREBP-1c) levels was notably up-regulated in HFD-vehicle mice (Fig. 7B,C) and was completely normalized by MSC and MSC-CM therapies. Beneficent transcriptional activity by forkhead box O1 (FoxO1) was suppressed in liver of HFD-vehicle mice and normalized by MSC and MSC-CM therapies (Fig. 7D). On the other hand, neither total cholesterol nor triglyceride levels were altered by MSC and MSC-CM therapies (Supporting Fig. 2A).

Resistin was densely stained in liver of HFD-vehicle mice and was reduced by MSC and MSC-CM therapies (Fig. 7E, top). Glucose transporter 2 (GLUT2) staining in the liver was reduced in liver of HFD-vehicle mice, but was recovered by MSC and MSC-CM therapies (Fig. 7E, bottom).

We also examined effects of MSC and MSC-CM therapies on serum adiponectin, insulin, and homeostasis model assessment-estimated IR (HOMA-IR) as major factors of IR. Serum adiponectin level was decreased in HFD-vehicle mice and normalized by MSC and MSC-CM therapies (Supporting Fig. 2B). The HOMA-IR level in the liver was significantly increased in HFD-vehicle mice and significantly reduced by MSC and MSC-CM therapies (Supporting Fig. 2B).

Discussion

We investigated the mechanism of action of MSC therapy for different pathological conditions in liver of HFD- and STZ-induced diabetic mice. Because only a limited number of donor MSCs were observed in the liver, we considered that the effects of the administered MSCs on damaged hepatocytes was a result of the humoral factors released from the MSCs. MSC-CM is a cocktail of various trophic factor secreted from MSCs. The present results show that the curative effects of the MSC and MSC-CM therapies on damaged hepatocytes in diabetic mice were similar: Both therapies ameliorated liver dysfunction and IR.

In previous studies reporting on effects of MSCs on hepatocyte damage, blood-glucose levels were recovered by pancreatic β-cell regeneration,[6,7] suggesting that

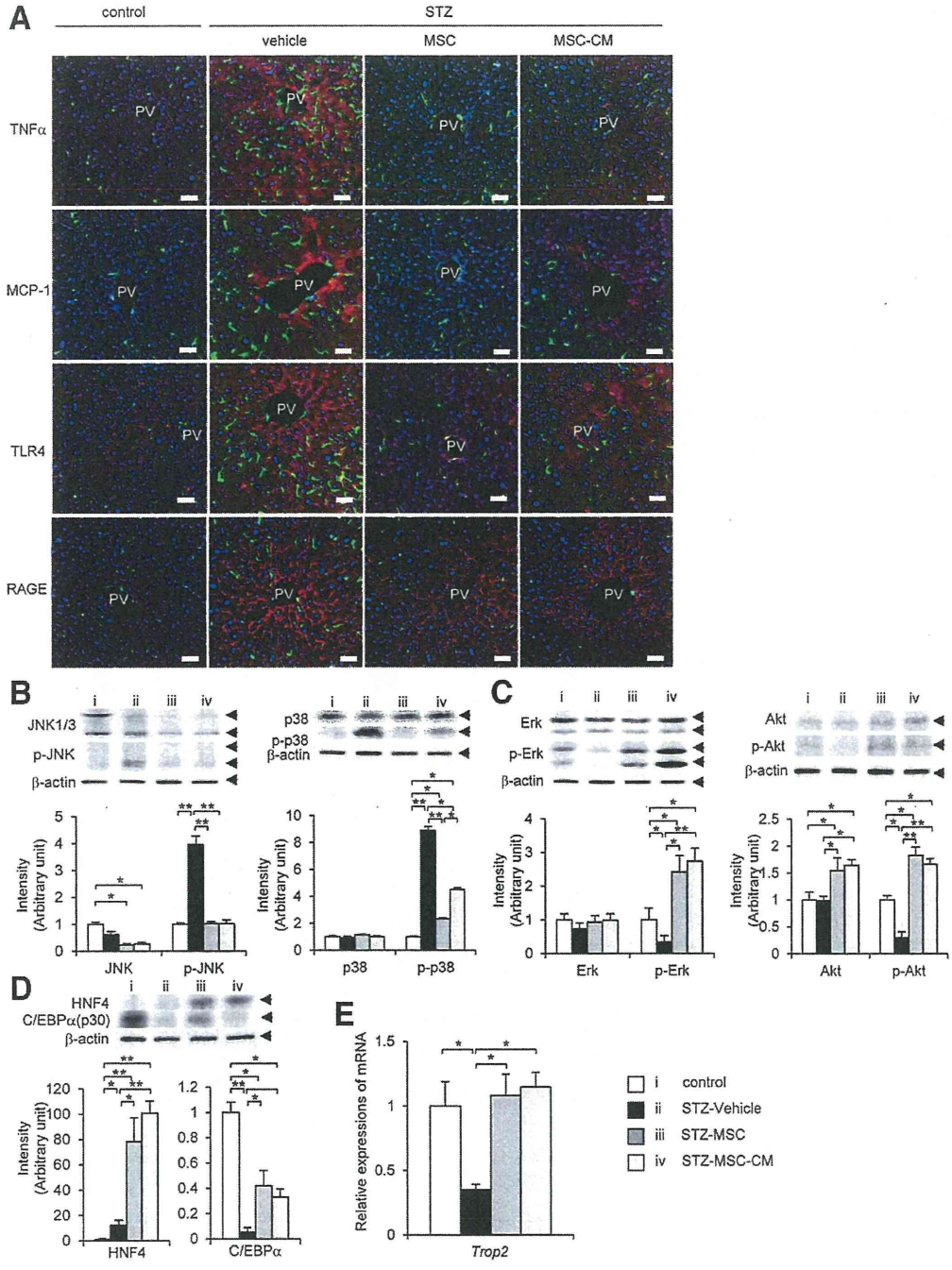

Fig. 6. Anti-inflammatory and proliferative effects and regenerative action of rMSCs and rMSC-CM therapies in liver of STZ-diabetic mice. (A) Immunofluorescence staining (red) of TNFα, MCP-1, TLR4, and receptor for advanced glycation endproducts (RAGE) in the liver. Bar, 50 μm. Protein levels of (B) JNK1/3, p-JNK, p38, p-p38, (C) Erk1/2, p-Erk, Akt, p-Akt, (D) HNF-4, and C/EBPα in liver of mice in each group. Relative amounts of protein are normalized to an internal control, β-actin. Intensity is shown as an arbitrary unit (n = 5, each group). (E) mRNA expression of *Trop2* in liver of each group (n = 5, each group). Relative amounts of mRNA are normalized to an internal control, β-actin. Data are expressed as mean ± SE values. $*P < 0.05$; $**P < 0.01$. mRNA, messenger RNA.

amelioration of hyperglycemia improves liver dysfunction. The present study revealed that even though hyperglycemia did not recover, diabetes-induced liver dysfunction was remarkably reversed by the MSC and MSC-CM therapies. The most interesting point was that hepatocyte regeneration occurred in the STZ-diabetic liver under persistent hyperglycemic conditions.

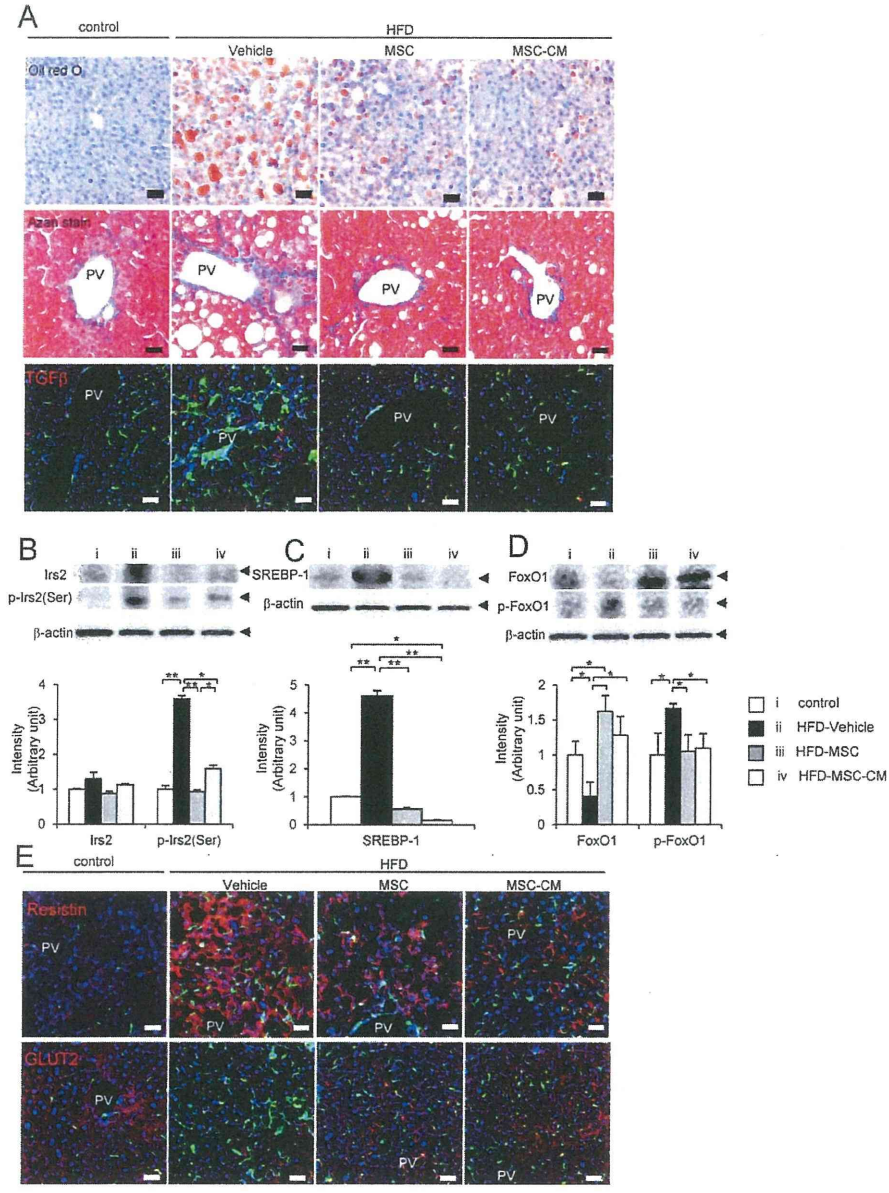

Fig. 7. Effects of rMSC and rMSC-CM therapies on lipogenesis, fibrosis, glucogenesis, and IR of liver in HFD-diabetic mice. (A) Oil Red O staining (top), Azan staining (middle), and TGF-β1 staining (bottom) in liver 8 weeks after initial treatment of MSC and MSC-CM. Lipid droplets are stained red and fibrosis are stained blue. Bar, 50 μm. Protein levels of (B) Irs2, abnormal phosphorylation of Irs2 serine^{723} (p-Irs2), (C) SREBP-1, (D) FoxO1, and phosphorylated FoxO1 (p-FoxO1) in liver of each group. Relative amounts of protein are normalized to an internal control, β-actin. Intensity is shown as an arbitrary unit (n = 5, each group). (E) Immunofluorescence staining (red) of resistin and GLUT2 in liver of each group. Bar, 50 μm. Data are expressed as mean ± SE values. $^*P < 0.05$; $^{**}P < 0.01$.

The present results showed a significant increase in BMDC infiltration into liver of HFD- and STZ-induced diabetic mice, which was completely reversed by the MSC and MSC-CM therapies. Macrophages are classified as classically activated macrophages (M1 macrophages) or as alternatively activated macrophages (M2 macrophages).[14] In this study, BMDCs in liver of diabetic mice displayed a molecular profile similar to that of proinflammatory M1 macrophages by expressing *Il-6* and *Cd11c*; however, they changed into M2 macrophages expressing *Fizz1* and *Mrc1* after application of the MSC and MSC-CM therapies. Further changes, including *Ccr2* expression, were also demonstrated in BMDCs in the liver and in mononuclear cells in the peripheral circulation. Expression of MCP-1 was stimulated in liver of diabetic mice, but was remarkably decreased by both therapies, suggesting that accelerated infiltration of BMDCs into the liver induced by MCP-1/CCR2 interactions was blocked by these treatments. ICAM-1 is induced in HSECs by cytokine or chemokine signals and enhances recruitment of inflammatory cells from vessels.[15] Here, notable expression of ICAM-1 in SECs contributed to excessive infiltration of BMDCs and was also suppressed by the MSC and MSC-CM therapies.

The present findings showed that both the MSC and MSC-CM therapies ameliorated inflammatory change and apoptotic reactions in hepatocytes caused

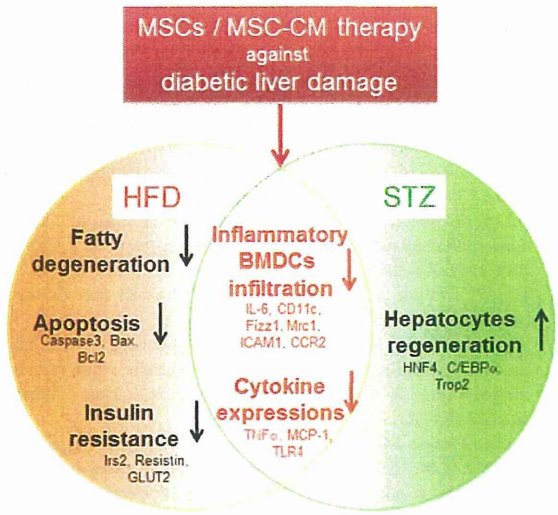

Fig. 8. Proposed mechanisms for therapeutic effects of MSCs and MSC-CM for type 2 and 1 diabetic liver damage. Effective mechanisms contribute to common, distinctive pathogenesis in liver of type 2 and 1 diabetes.

by HFD- and STZ-induced diabetes. Hyperlipidemia and hyperglycemia cause an increase in circulating endotoxins, which are ligands of TLR4.[16] In addition, hyperlipidemia and hyperglycemia induce transcription of proinflammatory cytokines, such as TNFα and MCP-1, and adipokines, such as FABP4, by nuclear translocation of NF-κB (nuclear factor kappa light-chain enhancer of activated B cells), which results in hepatic injury and IR.[17,18] FABP4 is known as a major adipokine that induces IR and is highly expressed in both adipose tissue and endothelial cells.[19,20] The liver is an important site for the clearance and catabolism of circulating advanced glycation endproducts.[21] Interaction of advanced glycation endproducts and their receptor induces NF-κB transcriptional activation and cytokine production by JNK and p38-MAPK activation.[22] On the other hand, activation of ERK1/2 and Akt induces hepatocyte proliferation, survival, and regeneration. These signaling pathways also regulate apoptosis of parenchymal cells by mitochondrial factors, such as Bax and Bcl-2, and caspase 3.[23] Therefore, in the present study, the inflammatory changes and apoptotic reactions in hepatocytes might have been the result of the following dual mechanism induced by the MSC and MSC-CM therapies: first through reduction of TLR4 expression and sequential inactivation of the p38-MAPK and JNK pathways and second through the direct effect of trophic factors derived from MSCs enhancing the ERK1/2 and Akt pathways.

Our MSC and MSC-CM therapies stimulated hepatocyte regeneration in STZ-diabetic mice. HNF-4 and C/EBPα are transcriptional factors that play a crucial role in the differentiation process of liver stem cells for fully functional mature hepatic cells.[24] Trop2 is not only a novel marker for oval cells, but also a regulator of cell-cell adhesion and cell-cycle progression through phosphorylation of ERK1/2.[25] The results showed that the MSC and MSC-CM therapies induced expression of HNF-4 and recovery of C/EBPα and *Trop2* in the STZ-diabetic liver, which might have activated progenitor cells for proliferation and functional recovery of hepatocytes. In contrast, none of the above effects were observed in HFD-diabetic mice, suggesting that the severe fatty degeneration of hepatocytes surpassed the regenerative potential (data not shown).

MSC and MSC-CM therapies not only reduced lipid accumulation in hepatocytes, but also prevented liver fibrosis. As previously reported, stellate cells in the liver are associated with liver fibrosis,[26] and activated stellate cells express TGF-β1.[27] Expression of TGF-β1 was up-regulated in HFD-vehicle mice and reversed by the MSC and MSC-CM therapies. Because almost 50% of BMDCs expressed TGF-β1, it was expected that liver fibrosis in HFD mice was induced by pathological BMDCs that had differentiated into stellate cells in the liver.

The MSC and MSC-CM therapies reversed hyperinsulinemia and down-regulated HOMA-IR in HFD-diabetic mice, suggesting that both therapies ameliorated insulin resistance. SREBP-1c and FoxO1 are master transacting factors that mediate lipogenesis, glucogenesis, lipid metabolism, and insulin sensitivity.[28,29] Resistin, an adipose-derived hormone, stimulates synthesis and secretion of proinflammatory cytokines, resulting in enhanced liver gluconeogenesis and inflammation.[30] GLUT2 is expressed in hepatocytes and regulates glucose uptake and glucose metabolism.[31] Adiponectin and its receptor are key components in IR that facilitate the translocation of GLUT2 through adenosine-monophosphate–activated protein kinase activation.[32] Here, MSC and MSC-CM therapies ameliorated IR by regulating expression of HOMA-IR, adiponectin, resistin, and proinflammatory cytokines.

Taken together, we demonstrated that MSC and MSC-CM therapies are powerful tools for repairing diabetes-induced hepatocyte damage in HFD- and STZ-diabetic mice and sequential IR in HFD-diabetic mice (Fig. 8). In STZ-diabetic mice, neither therapy induced β-cell regeneration immediately after MSC therapy; instead, they induced hepatocyte regeneration, despite having been conducted under hyperglycemic conditions. Effects of MSC cell therapy might be the result of MSC-derived trophic factors. We speculate

that the mechanism of hepatocyte damage repair in diabetes may involve various factors that regulate immune reaction, lipogenesis, glucogenesis, and regeneration of hepatocytes (Fig. 8). MSC therapy with such a pleiotropic action is an effective treatment for diabetic liver damage and may open the door for a novel remedy.

Acknowledgment: The authors thank J. Yanagawa, K. Kamiya, and Y. Hayakawa, research assistants in the Second Department of Anatomy, and K. Fujii, research assistant in the First Department of Internal Medicine, for their technical assistance.

References

1. Brunt EM, Janney CG, Di Bisceglie AM, Neuschwander-Tetri BA, Bacon BR. Nonalcoholic steatohepatitis: a proposal for grading and staging the histological lesions. Am J Gastroenterol 1999;94:2467-2474.
2. West J, Brousil J, Gazis A, Jackson L, Mansell P, Bennett A, Aithal GP. Elevated serum alanine transaminase in patients with type 1 or type 2 diabetes mellitus. QJM 2006;99:871-876.
3. Kojima H, Fujimiya M, Matsumura K, Nakahara T, Hara M, Chan L. Extrapancreatic insulin-producing cells in multiple organs in diabetes. Proc Natl Acad Sci U S A 2004;101:2458-2463.
4. Fujimiya M, Kojima H, Ichinose M, Arai R, Kimura H, Kashiwagi A, Chan L. Fusion of proinsulin-producing bone marrow-derived cells with hepatocytes in diabetes. Proc Natl Acad Sci U S A 2007;104:4030-4035.
5. Terashima T, Kojima H, Fujimiya M, Matsumura K, Oi J, Hara M, et al. The fusion of bone-marrow-derived proinsulin-expressing cells with nerve cells underlies diabetic neuropathy. Proc Natl Acad Sci U S A 2005;102:12525-12530.
6. Bell GI, Broughton HC, Levac KD, Allan DA, Xenocostas A, Hess DA. Transplanted human bone marrow progenitor subtypes stimulate endogenous islet regeneration and revascularization. Stem Cells Dev 2012;21:97-109.
7. Anzalone R, Lo Iacono M, Loria T, Di Stefano A, Giannuzzi P, Farina F, La Rocca G. Wharton's jelly mesenchymal stem cells as candidates for beta cells regeneration: extending the differentiative and immunomodulatory benefits of adult mesenchymal stem cells for the treatment of type 1 diabetes. Stem Cell Rev 2011;7:342-363.
8. Ezquer M, Ezquer F, Ricca M, Allers C, Conget P. Intravenous administration of multipotent stromal cells prevents the onset of non-alcoholic steatohepatitis in obese mice with metabolic syndrome. J Hepatol 2011;55:1112-1120.
9. Si Y, Zhao Y, Hao H, Liu J, Guo Y, Mu Y, et al. Infusion of mesenchymal stem cells ameliorates hyperglycemia in type 2 diabetic rats: identification of a novel role in improving insulin sensitivity. Diabetes 2012;61:1616-1625.
10. Prockop DJ, Oh JY. Mesenchymal stem/stromal cells (MSCs): role as guardians of inflammation. Mol Ther 2012;20:14-20.
11. Kuroda Y, Kitada M, Wakao S, Dezawa M. Bone marrow mesenchymal cells: how do they contribute to tissue repair and are they really stem cells? Arch Immunol Ther Exp (Warsz) 2011;59:369-378.
12. van Poll D, Parekkadan B, Cho CH, Berthiaume F, Nahmias Y, Tilles AW, Yarmush ML. Mesenchymal stem cell-derived molecules directly modulate hepatocellular death and regeneration in vitro and in vivo. HEPATOLOGY 2008;47:1634-1643.
13. Javazon EH, Colter DC, Schwarz EJ, Prockop DJ. Rat marrow stromal cells are more sensitive to plating density and expand more rapidly from single-cell-derived colonies than human marrow stromal cells. Stem Cells 2001;19:219-225.
14. Gordon S. Alternative activation of macrophages. Nat Rev Immunol 2003;3:23-35.
15. Arii S, Imamura M. Physiological role of sinusoidal endothelial cells and Kupffer cells and their implication in the pathogenesis of liver injury. J Hepatobiliary Pancreat Surg 2000;7:40-48.
16. Shi H, Kokoeva MV, Inouye K, Tzameli I, Yin H, Flier JS. TLR4 links innate immunity and fatty acid-induced insulin resistance. J Clin Invest 2006;116:3015-3025.
17. Tilg H. The role of cytokines in non-alcoholic fatty liver disease. Dig Dis 2010;28:179-185.
18. Solomon SS, Odunusi O, Carrigan D, Majumdar G, Kakoola D, Lenchik NI, Gerling IC. TNF-alpha inhibits insulin action in liver and adipose tissue: A model of metabolic syndrome. Horm Metab Res 2010;42:115-121.
19. Queipo-Ortuno MI, Escote X, Ceperuelo-Mallafre V, Garrido-Sanchez L, Miranda M, Clemente-Postigo M, et al. FABP4 dynamics in obesity: discrepancies in adipose tissue and liver expression regarding circulating plasma levels. PLoS One 2012;7:e48605.
20. Maeda K, Cao H, Kono K, Gorgun CZ, Furuhashi M, Uysal KT, et al. Adipocyte/macrophage fatty acid binding proteins control integrated metabolic responses in obesity and diabetes. Cell Metab 2005;1:107-119.
21. Sebekova K, Kupcova V, Schinzel R, Heidland A. Markedly elevated levels of plasma advanced glycation end products in patients with liver cirrhosis—amelioration by liver transplantation. J Hepatol 2002;36:66-71.
22. Yeh CH, Sturgis L, Haidacher J, Zhang XN, Sherwood SJ, Bjercke RJ, et al. Requirement for p38 and p44/p42 mitogen-activated protein kinases in RAGE-mediated nuclear factor-kappaB transcriptional activation and cytokine secretion. Diabetes 2001;50:1495-1504.
23. Pradelli LA, Beneteau M, Ricci JE. Mitochondrial control of caspase-dependent and -independent cell death. Cell Mol Life Sci 2010;67:1589-1597.
24. Nagaki M, Moriwaki H. Transcription factor HNF and hepatocyte differentiation. Hepatol Res 2008;38:961-969.
25. Okabe M, Tsukahara Y, Tanaka M, Suzuki K, Saito S, Kamiya Y, et al. Potential hepatic stem cells reside in EpCAM+ cells of normal and injured mouse liver. Development 2009;136:1951-1960.
26. Sakaida I, Nagatomi A, Hironaka K, Uchida K, Okita K. Quantitative analysis of liver fibrosis and stellate cell changes in patients with chronic hepatitis C after interferon therapy. Am J Gastroenterol 1999;94:489-496.
27. Fujimiya T, Liu J, Kojima H, Shirafuji S, Kimura H, Fujimiya M. Pathological roles of bone marrow-derived stellate cells in a mouse model of alcohol-induced fatty liver. Am J Physiol Gastrointest Liver Physiol 2009;297:G451-G460.
28. Ide T, Shimano H, Yahagi N, Matsuzaka T, Nakakuki M, Yamamoto T, et al. SREBPs suppress IRS-2-mediated insulin signalling in the liver. Nat Cell Biol 2004;6:351-357.
29. Matsumoto M, Han S, Kitamura T, Accili D. Dual role of transcription factor FoxO1 in controlling hepatic insulin sensitivity and lipid metabolism. J Clin Invest 2006;116:2464-2472.
30. Muse ED, Obici S, Bhanot S, Monia BP, McKay RA, Rajala MW, et al. Role of resistin in diet-induced hepatic insulin resistance. J Clin Invest 2004;114:232-239.
31. Burcelin R, Dolci W, Thorens B. Glucose sensing by the hepatoportal sensor is GLUT2-dependent: in vivo analysis in GLUT2-null mice. Diabetes 2000;49:1643-1648.
32. Kadowaki T, Yamauchi T, Kubota N, Hara K, Ueki K, Tobe K. Adiponectin and adiponectin receptors in insulin resistance, diabetes, and the metabolic syndrome. J Clin Invest 2006;116:1784-1792.

Biochemical and Biophysical Research Communications 407 (2011) 557–561

Contents lists available at ScienceDirect

Biochemical and Biophysical Research Communications

journal homepage: www.elsevier.com/locate/ybbrc

An Mdm2 antagonist, Nutlin-3a, induces p53-dependent and proteasome-mediated poly(ADP-ribose) polymerase1 degradation in mouse fibroblasts

Shingo Matsushima [1], Naoyuki Okita [*,1], Misako Oku, Wataru Nagai, Masaki Kobayashi, Yoshikazu Higami [*]

Department of Molecular Pathology and Metabolic Disease, Faculty of Pharmaceutical Sciences, Tokyo University of Science, Yamazaki 2641, Noda, Chiba 278-0022, Japan

ARTICLE INFO

Article history:
Received 10 March 2011
Available online 16 March 2011

Keywords:
Nutlin-3a
Poly(ADP-ribose) polymerase1
p53
Mdm2
Proteasome

ABSTRACT

Nutlin-3a (Nutlin) is an Mdm2 inhibitor and is potent to stabilize p53, which is a tumor-suppressor involved in various biological processes such as cell cycle regulation, DNA repair, and apoptosis. Here we demonstrate that Nutlin treatment in mouse fibroblast cell lines reduces the protein levels of poly(ADP-ribose) polymerase1 (Parp1). Parp1 functions in DNA repair, replication, and transcription and has been regarded as a target molecule for anti-cancer therapy and protection from ischemia/reperfusion injury. In this study, first we found that Nutlin, but not DNA damaging agents such as camptothecin (Cpt), induced a decrease in the Parp1 protein levels. This reduction was not associated with cell death and not observed in p53 deficient cells. Next, because Nutlin treatment did not alter Parp1 mRNA levels, we expected that a protein degradation pathway might contribute to this phenomenon. Predictably, a proteasome inhibitor, MG132, inhibited the Nutlin-induced decrease in the levels of Parp1 protein. These results show that Nutlin induces the proteasomal degradation of Parp1 in a p53-dependent manner. Thus, this study demonstrates characterization of a novel regulatory mechanism of Parp1 protein. This novel regulatory mechanism of Parp1 protein level could contribute to development of inhibitors of the Parp1 signaling pathway.

1. Introduction

p53 is a tumor-suppressor that is mutated or deleted in more than half of all human tumors. The physiological roles of p53 are versatile, forming a cell cycle checkpoint and functioning in DNA repair, apoptosis, and energy metabolism [1]. It has been shown that phosphorylations at multiple sites and subsequent proteasomal degradation are important in the regulation of p53 protein levels [2]. p53 ubiquitination required in its degradation is catalyzed by several ubiquitin ligases such as Mdm2, Pirh2, and Cop1 [3]. In particular, the regulatory mechanism of p53 by Mdm2 has been well-analyzed. Because the massive stabilization of p53 was able to induce apoptosis in p53 proficient tumor cells [4], stabilization of p53 via an inhibition of Mdm2 is one of the attractive strategies for cancer therapy. Recently, it has been reported that small molecular compounds such as Nutlin and MI-219 act as cell-permeable Mdm2 antagonists [5,6], and their analogs have progressed to preclinical development or early phase clinical trials for anti-cancer therapy [7].

Parp1 is a major enzyme catalyzing poly(ADP-ribosyl)ation, which is a post-translational protein modification. It is involved in replication, DNA repair, and cell death [8,9]. Parp1 is dramatically activated by DNA breaks and then catalyzes poly(ADP-ribosyl)ation on substrate proteins in DNA damage regions, which is required for efficient recruitment of DNA repair factors to the loci [10,11]. On the other hand, over-activation of Parp1 decreases cellular NAD^+ and ATP levels, resulting in necrotic cell death caused by breakdown of energy metabolism [12,13]. The involvement of Parp1 in inflammatory responses has also been reported. Ischemia/reperfusion-induced Parp1 over-activation is mediated by production of reactive oxygen species and is involved in NF-κB transactivation [14]. Furthermore, Parp1 has been also characterized as a useful hallmark of apoptosis because full length Parp-1 is cleaved by the apoptotic proteases, caspase-3 and -7, into p85 and p25 fragments during apoptosis [15,16]. Therefore, Parp1 is an attractive target of cancer chemotherapy and protection from ischemia/reperfusion injury, and several Parp1 inhibitors are being evaluated in clinical trials [17].

Recently, using Nutlin, we have analyzed p53 functions that are independent of DNA damage response and incidentally found that Parp1 proteins disappear in Nutlin-treated cells. In this study, we show the basic characterization of Nutlin-mediated Parp1 protein degradation and discuss the use of Nutlin as a Parp1 inhibitor for protection against ischemia/reperfusion injury and anti-cancer therapy.

* Corresponding authors. Fax: +81 4 7121 3676..
E-mail addresses: nokita7@rs.noda.tus.ac.jp (N. Okita), higami@rs.noda.tus.ac.jp (Y. Higami).
[1] These authors equally contributed to this work.

0006-291X/$ - see front matter © 2011 Elsevier Inc. All rights reserved.
doi:10.1016/j.bbrc.2011.03.061

2. Materials and methods

2.1. Cell culture and drugs

Mouse fibroblast cell line 3T3-L1 and 3T3-F442A were purchased from the RIKEN Bioresource Center (Japan) and the European Collection of Animal Cell Cultures (UK), respectively. p53 deficient mouse-derived fibroblast cell line HW [18] was kindly provided by Dr. Masayuki Saito (Tenshi University, Japan). The cells were maintained in Dulbecco's modified Eagle's medium (low glucose) (WAKO, Japan) with 10% fetal calf serum and 1% penicillin/streptomycin (SIGMA). Cpt and MG132 were purchased from WAKO (Japan). Nutlin was supplied by Cayman (USA).

2.2. p53 overexpression and knockdown

p53 cDNA was amplified from mouse liver cDNA by PCR using KOD plus (TOYOBO, Japan) and subcloned into EcoRV-digested pBluescript II SK(+). And then p53 cDNA fragment obtained by BamHI and DraI digestion of the subcloned vector were cloned into EcoRV and BamH1-digested pIRES-Neo3 (Clontech, USA). The produced vector, p53-IRES-Neo3, was transfected with Lipofectamine LTX (Invitrogen, USA) into 3T3-L1 cells, according to the manufacturer's protocol.

We designed a mouse p53 shRNA expression vector based on target sequences for effective p53 knockdown, as previously reported [19]. Two oligonucleotides, 5′-gatccccGTACGTGTGTAGTA GCTTCttcaagagaGGAGCTATTACACATGTACtttttggaaa-3′ and 5′-agc ttttccaaaaaGTACATGTGTAATAGCTCCtctcttgaaGAAGCTACTACACAC GTACggg -3′ (upper case letters, target sequences against p53; lower case letters, BglII, HindIII or loop structure sequences) were chemically synthesized (Operon Biotechnology, USA). The annealed oligos were directly ligated into a BglII and HindIII-digested pSUPER-puro shRNA expression vector gifted from Dr. Shigeo Ohno (Yokohama City University, Japan) [20]. The produced vector, termed pSUPER-puro-shmp53, was transfected with Lipofectamine LTX (Invitrogen, USA) into 3T3-L1 cells, according to the manufacturer's protocol. For stable p53 knockdown cell lines, the transfected cells were selected with puromycin and resistant clones were isolated by trypsinization using cloning cylinders.

2.3. Preparation of primary mouse embryonic fibroblasts (MEFs)

p53 heterozygous mice (Accession No. CDB 0001K) [21] were purchased from RIKEN BRC (Japan). p53 heterozygous males and females were crossed, and MEFs were prepared from the pregnant females. Each 13- to 15-day-old embryo was dissected from the uterus and washed with PBS. After removal of the head, tail, limbs, and blood-enriched organs, the trimmed embryo was washed with PBS and minced. After trypsinization at 37 °C for 10 min followed by inactivation of trypsin by addition of FCS, MEFs were separated by filtration through a cell-strainer. p53 status was confirmed by PCR using previously described primers (forward primer for p53 genomic sequence, 5′-AATTGACAAGTTATGCATCCAACAGTACA-3′; reverse primer for p53 genomic sequence, 5′-ACTCCTCAACATC CTGGGGCAGCAACAGAT-3′, forward primer for neo sequence, 5′-GAACCTGCGTGCAATCCATCTTGTTCAATG-3′) [21] and the established MEFs were maintained in DMEM high glucose with 10% FCS, 2-mercaptoethanol (2-ME), and antibiotics.

2.4. Western blotting

Cells were lyzed by the addition of lysis buffer (50 mM Tris–HCl pH6.8, 2% SDS, 5% glycerol), boiled for 5 min, and sonicated. Protein concentrations of the soluble fraction were determined by BCA protein assay (PIERCE, USA) according to the manufacturer's protocol, and standardized by the addition of lysis buffer. Following this, the proteins were added to 2-ME and bromophenol blue so as to obtain final concentrations of 5% and 0.025%, respectively, and boiled for 5 min. Equal amounts of proteins (5–20 μg) were subjected to SDS–PAGE and transferred to nitrocellulose membranes. The membranes were blocked with 2.5% skim milk and 0.25% BSA in TBS (50 mM Tris, pH 7.4, 150 mM NaCl) containing 0.1% Tween 20 (TTBS) for 1 h at room temperature, and then probed with appropriate primary antibodies overnight at 4 °C or for 2 h at room temperature. As primary antibodies, anti-Parp1 (clone C-2-10, WAKO, Japan), anti-p53 (clone Ab-1, Calbiochem, USA), anti-b actin (clone AC-15, SIGMA, USA), or anti-caspase-3 (clone 1F3, MBL, Japan) antibodies were used. After washes with TTBS, the membranes were incubated with the appropriate secondary antibody, horseradish peroxidase-conjugated $F(ab')_2$ fragment of goat anti-mouse IgG or anti-rabbit IgG (Jackson Immunoresearch, USA), for 1 h at room temperature. After washing the membrane with TTBS, the membranes were incubated with ImmunoStar LD reagent (WAKO, Japan). The specific proteins were visualized with LAS3000 (FUJI FILM, Japan), and the data were analyzed using MultiGauge software (FUJI FILM, Japan).

2.5. RNA purification and RT-PCR

Cells were lyzed by RNAiso PLUS (TaKaRa, Japan), and then total RNA was purified using a FastPure RNA kit (TaKaRa, Japan) according to manufacturer's protocol. Purified RNA (1 μg) was subjected to reverse transcription with PrimeScript Reverse Transcriptase (TaKaRa, Japan) and random hexamer (TaKaRa, Japan). The PCR reaction was performed using Platinum Taq DNA Polymerase High Fidelity (Invitrogen, USA) and *Parp1* (forward, 5′-TGCTCATCTT CAACCAGCAG-3′; reverse, 5′-TCCTTTGGAGTTACCCATTCC-3′) or β-*actin* primers (forward, 5′-TCTTTGCAGCTCCTTCGTTG-3′; reverse, 5′-GGCCTCGTCACCCACATAG-3′) as follows: initiation step, at 94 °C for 1 min; amplification step, 30 (*Parp-1*) or 25 (*b-actin*) cycles of at 94 °C for 1 min, at 52 °C (*Parp-1*) or 61 °C (β-*actin*) for 15 s, at 68 °C for 15 s; termination step, 68 °C 15 s. PCR products were subjected to 1.8% agarose gel electrophoresis, stained with ethidium bromide, and visualized with LAS3000. The data was analyzed using MultiGauge software (FUJI FILM, Japan).

3. Results

3.1. Nutlin induces a decrease in parp1 protein levels in mouse fibroblast cell lines

When analyzing proteins of the Nutlin-treated mouse embryonic fibroblasts (MEFs), we observed a significant reduction in the levels of full length of Parp1 protein without cleavage into p85 and p25 apoptotic fragments (data not shown). Interestingly, under this condition, a trypan blue exclusion assay and images of phase-contrast microscope showed that the cells were viable, suggesting that the reduction of Parp1 protein was independent of cell death. Furthermore, because MEFs were induced apoptosis by staurosporine treatment, MEFs were responsive to apoptotic stimuli (data not shown). To examine whether p53 stabilization induces the decrease in Parp1 protein, 3T3-L1 and 3T3-F442A mouse fibroblast cells were treated with a DNA damaging agent, Cpt, or Nutlin. As shown in Fig. 1A and B, in both cell lines, Cpt treatment did not alter the Parp-1 protein levels, and Nutlin markedly decreased it, although both drugs induced p53 stabilization. Furthermore, overexpression of p53 protein did not markedly affect Parp1 protein levels (Fig. 1C). Consistent with our previous observations, no caspase-3 activation, which is a hallmark of apop-

tosis, was detected in these conditions. Furthermore, trypan blue staining showed that the Nutlin treatment did not induced cell death (Supplementary data Fig. 1). The time course analysis showed that Parp1 protein diminished by a treatment with 25 μM Nutlin for 8 h (Fig. 1D). These results suggest that in mouse fibroblasts Nutlin induces the reduction of Parp1 protein in a cell death-independent manner.

3.2. p53 Mediates Nutlin-induced decrease in parp1 protein

Since Nutlin stabilizes p53 *via* inhibition of Mdm2, we examined whether p53 contributes to the Nutlin-induced Parp-1 reduction. shRNA-mediated transient knockdown of p53 in 3T3-L1 cells attenuated the decrease in Parp1 by Nutlin treatment (Fig. 2A). Since p53 knockdown efficiency is not sufficient, we next analyzed this using two p53 deficient cell lines. 3T3-L1/shp53 cells were established by stable transfection with the pSUPER-puro-shmp53 plasmid vector followed by clone isolation, and its p53 protein expression levels were very much lower than in the transient knockdown. HW cells are a fibroblast cell line derived from p53 deficient mice. In these cell lines, the Nutlin-induced decrease in Parp1 was diminished significantly (Fig. 2B). Furthermore, we confirmed p53 dependency in the Nutlin-induced Parp1 reduction by using MEFs derived from p53+/+ or −/− mice, and obtained similar results (Fig. 2C). These results show that Nutlin reduces the Parp1 protein levels in a p53-dependent manner.

3.3. Nutlin-3 down-regulates parp-1 protein via proteasome

To examine whether the decrease in Parp1 protein by Nutlin treatment is caused by down-regulation of its mRNA, p53 proficient (3T3-L1 and 3T3-F442A) and deficient (3T3-L1/shp53 and HW) cell lines were treated with Nutlin, and then the Parp1 mRNA of each was analyzed by RT-PCR. Parp1 mRNA did not markedly change in either p53 proficient or deficient cell lines, even at doses of Nutlin where levels of Parp1 protein were completely dimin-

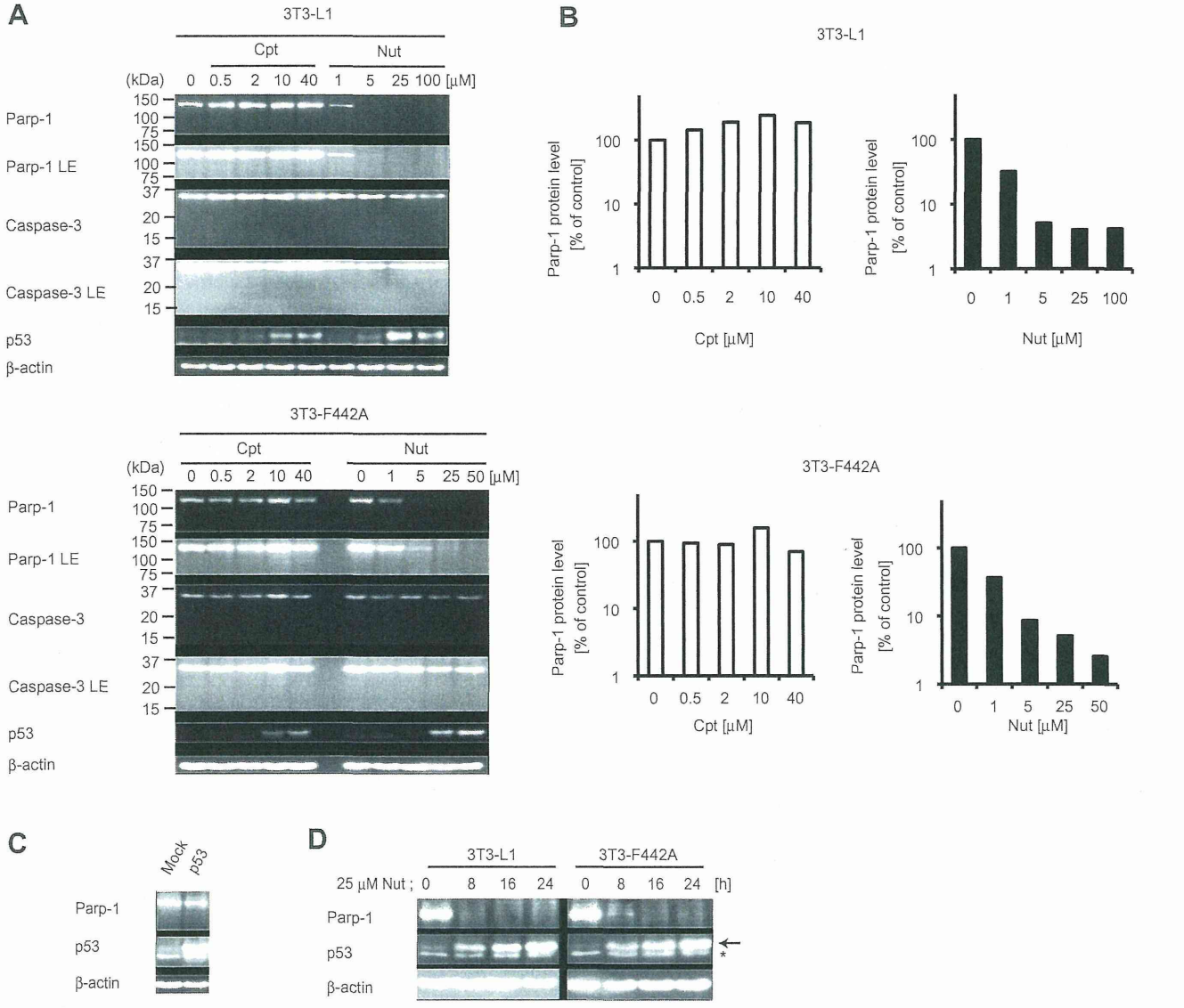

Fig. 1. Nutlin but not Cpt induces decrease in Parp1 protein levels in mammalian cell lines. A and B, mouse fibroblast 3T3-L1 (upper panel) or 3T3-F442A (lower panel) cells were treated with indicated concentrations of Cpt or Nutlin for 24 h. The cell lysates were analyzed by Western blotting using indicated antibodies (A). LE means long exposure. Quantitative data from (A) are shown (B). C, 3T3-L1 cells were transfected with mock or p53 expression vector. After transfection for 36 h, the cells were harvested and were analyzed by western blotting using indicated antibodies. D, 3T3-L1 or 3T3-F442A cells were treated with 25 μM Nutlin for the indicated times. Proteins were subjected to Western blotting. In the p53 panel, the arrow and asterisk show the p53 and nonspecific bands, respectively. All experiments were performed at least three times, and representative data are shown.

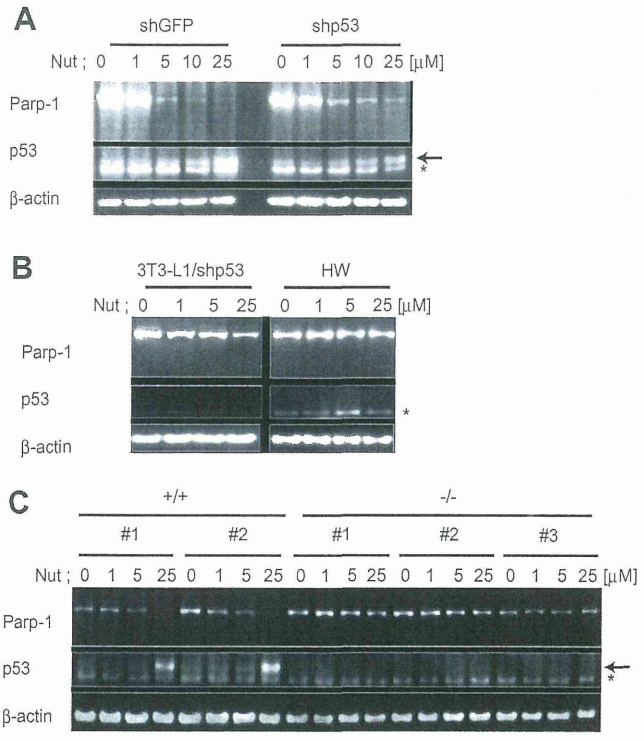

Fig. 2. Decrease in Parp1 protein levels induced by Nutlin is p53 status dependent. shGFP- and shp53- transiently transfected 3T3-L1 (A), HW, a mouse fibroblast cell line from p53 knockout mice, and 3T3-L1/shp53, a p53 stable knockdown cell line (B), and p53+/+ ($n = 2$) and p53−/− ($n = 3$) MEFs (C) were treated with indicated concentrations of Nutlin for 24 h. The cell lysates were analyzed by Western blotting using indicated antibodies. In the p53 panel, the arrow and asterisk show the p53 and nonspecific bands, respectively. All experiments were performed at least two times, and representative data are shown.

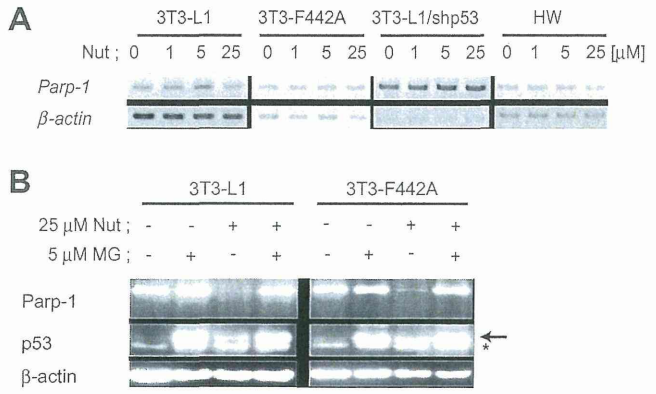

Fig. 3. Nutlin downregulates Parp-1 protein levels by proteasomal degradation. A, 3T3-L1, 3T3-F442A, 3T3-L1/shp53, and HW cells were treated with the indicated concentrations of Nutlin for 24 h. Parp1 mRNA was detected by RT-PCR. β-actin was used as a loading control. B, 3T3-L1 and 3T3-F442A cells were treated with 25 mM Nutlin in the presence or absence of 5 μM proteasome inhibitor MG132 (MG) for 8 h, and then the cell lysates were subjected to Western blotting using indicated antibodies. All experiments were performed at least three times, and representative data are shown.

ished (Fig. 3A). This result indicates that a decrease in Parp1 mRNA levels is not a main factor of Nutlin-induced Parp1 reduction. Therefore, we speculated that Nutlin-induced Parp1 reduction might involve proteasomal degradation. Thus, the effects of proteasome inhibition on Nutlin-induced Parp1 reduction were examined. Treatment with the proteasome inhibitor MG132 alone did not affect basal Parp1 protein levels, but it clearly inhibited the Nutlin-induced reduction in Parp1 (Fig. 3B). Taken together, these results indicate that the Nutlin treatment induced proteasome-mediated degradation of Parp-1 protein.

4. Discussion

In this study, we demonstrated that the Mdm2 inhibitor, Nutlin, induces the reduction of Parp1 protein by a p53-dependent mechanism. Interestingly, overexpression of p53 protein did not evoke a significant reduction in Parp1 protein, although that induced p53 accumulation similar to Nutlin. These results suggest that in the process of Nutlin-induced Parp1 reduction, p53 expression is required but is insufficient.

We examined whether the other commercially available Mdm2 inhibitors (NSC66811 [22] and trans-4-Iodo, 4′-boranyl-chalcone [23,24]) induced a reduction in Parp1 protein in 3T3-L1 cells. However, these Mdm2 inhibitors not only did not induce a reduction in Parp1 protein but also did not induce even p53 accumulation (data not shown). To conclude this issue, additional experiments would be required. We also showed that MG132 blocks the decrease in Parp1 protein. It was reported that Parp1 can be ubiquitinated *in vivo*, although it is unclear whether the ubiquitination is involved in proteasomal degradation of Parp1 [25]. Taken together with our findings, it is likely that the ubiquitin–proteasome pathway directly regulates the degradation of Parp1 protein.

In comparison to the many Parp1 inhibitors evaluated in ongoing clinical trials [17], the regulatory mechanism of Parp1 protein that we discovered provides some advantages. The first advantage is the novel mechanism of action as an inhibitor of the Parp1 signaling pathway. Because most of the Parp1-inhibiting compounds previously identified block the catalyzing activity of the protein, the specificity of these drugs in the other Parp family proteins that possess the highly conserved catalytic domain is a big issue [17]. On the other hand, Nutlin inhibits Parp1 signaling *via* induction of Parp1 protein degradation. Therefore, we expect that the inhibition specificity for Parp1 protein in the Parp family could be high. In any case, it is important to analyze the effects of Nutlin treatment on the protein levels of the other Parp family proteins. The second advantage is its cell type selectivity. In this paper, we demonstrated that in mouse fibroblasts Nutlin induces the decrease in Parp1 protein. On the other hand, it has been reported that Nutlin induces cleavage of Parp1 into two apoptotic fragments in the human colon cancer cell line, HCT116, and the human myeloid leukemia cell line, ML-1 [26,27]. In fact, we confirmed that there was no significant reduction in Parp1 protein other than apoptotic cleavage in HCT116 cells treated with various doses of Nutlin (data not shown). Furthermore, we have already examined responsiveness to Nutlin-induced Parp1 decrease in several human cell lines and have confirmed that human lung cancer cell line A549 were also responsive to Nutlin (data not shown). Taken together, we believe that Nutlin-induced Parp1 degradation has cell type selectivity. Moreover, considering co-treatment with DNA damaging agents for cancer therapy, Nutlin may reduce side effects caused by DNA damaging agents. It is well known that alkylating agents cause Parp1 over-activation, resulting in massive inflammation due to undesirable necrotic cell death caused by NAD^+ and ATP depletion [12,13], and that Parp1 is required for NF-κB transactivation, which is involved in inflammatory responses [14]. Therefore, co-treatment with Nutlin may also attenuate necrotic cell death and inflammation induced by Parp1 over-activation.

Thus, this study demonstrates characterization of a novel regulatory mechanism of Parp1 protein. The elucidation of the regulatory mechanism of Nutlin-induced elimination of Parp1 protein is important for the optimization of compounds inducing this phenomenon, resulting in establishment of selective chemotherapeutic strategies against ischemia/reperfusion injury and cancer.